Biophysical Chemistry 17 (1983) 245–258
Elsevier Biomedical Press

ENTROPY EFFECTS ON THE ION-DIFFUSION RATE IN TRANSMEMBRANE PROTEIN CHANNELS

Jürgen BRICKMANN and Walter FISCHER

Institut für Physikalische Chemie, Technische Hochschule Darmstadt, Petersenstr. 20, D-6100 Darmstadt, F.R.G

Received 31st August 1982
Revised manuscript received 26th November 1982
Accepted 7th December 1982

Key words: Ion diffusion; Entropy effect; Ion channel; Biological membrane

We treat the transport of univalent cations through pore-like protein channels in biological membranes analytically, using two models (A + B) for the channel and the ion-channel interaction. A Lennard-Jones-type repulsion between the ions and the pore wall is introduced. We also include Van der Waals- and coulomb-type interactions between polar ligands of the pore-forming protein (e.g., carbonyl groups directed towards the axis of the channel) and the migrating particles. In model A, the polar groups are assumed to occur in pairs of dipoles pointing in opposite directions (as in the gramicidin A channel), while in model B the channel is treated as a pore with a radially isotropic charge distribution. In both models the ion-channel interaction leads to the occurrence of periodic potentials, corresponding to quasi-equilibrium and transition state sites of the ion in the pore. The diffusion rate can be calculated employing rate-theoretical concepts on the basis of microscopic parameters. It is demonstrated that the anomaly (inversion of the normal mass effect) for the transport rates of different ions can be related to differences in the activation entropy. The latter quantity is estimated analytically for both models. As a test, we performed numerical calculations with parameters based on the gramicidin A model. The results are in good agreement with experimental data and data from computer simulations. This shows that simple analytic expressions are well suited for predicting trends in the ionic conductivity of protein channels on the basis of microscopic interactions.

1. Introduction

There is now considerable evidence that cation diffusion through biological membranes takes place via transport mechanisms which are totally different from those of ion diffusion in aqueous solution. The ions can be transported by carrier molecules across the membrane or can migrate directly through pore-like protein channels. The latter mechanism is examined in the present work. It is well known from a variety of experimental [1–8] and theoretical investigations [9–13] that ion transport through membrane channels can be treated within rate-theoretical models. In these models, the overall transport rate is the product of three different contributions: the association (dehydration) of the ion with the channel, its transport from one end of the channel to the other (migration), and the dissociation (hydration) of the ion from the channel to the liquid. Since the geometrical parameters of ion channels in biomembranes are of the order of magnitude of the diameter of small molecules, there is no a priori justification for using concepts appropriate to a free liquid to describe transport phenomena. Each of the three main steps (dehydration, migration, hydration) has to be studied from a microscopic point of view. Each of them can substantially contribute to ion-specific transport properties. The subject of this paper is related to the migration in the channel interior. In particular, the influence of structural inhomogeneities of the channel on the migration rate of different ions is studied. In general, real protein channels have a highly complicated structure and a detailed analysis of the influence of microscopic interaction between the

0301-4622/83/0000–0000/$03.00

penetrating particle (ion, ion plus water molecules) and the molecular groups forming the channel is not possible as a consequence of a substantial lack of microscopic information. However, the situation is much better for a model channel formed by a dimer of the gramicidin A molecule, the structure of which is well known [14,15] and for which much experimental information on the ion-diffusion rate through single channels is available [2,3,16,17]. This model channel has a helical structure with a central tunnel with a diameter of about 4 Å. A single ion or an ion-water complex passing through the channel will interact primarily with the peptide carbonyl groups of the gramicidin A molecule, since these groups have a high polarity causing a strong coulombic interaction with the cation, and since the CO groups are closest to the channel axis. There are six carbonyl groups in a single turn of the molecular helix directed towards its axis with an angle of about 20° with respect to the axis. The orientation of these groups alternates, producing a periodic potential for the ion migrating along the helix axis.

The detailed information available for the gramicidin A channel allows the study of the ion-transport mechanism from a microscopic point of view, at least on the basis of simplifying model assumptions. The results of first attempts towards this goal were recently presented by Fischer et al. [18]. The authors performed molecular dynamics calculations for the ion migration on the axis of the helix assuming pure electrostatic interactions between the ion and flexible carbonyl groups. It was demonstrated that the molecular dynamics results are in good agreement with those obtained from the rate theory analysis of Läuger and co-workers [9,19]. However, no conclusions which lead to an understanding of the selectivity effects and anomalous diffusion behaviour found experimentally by Neher and co-workers [2,3] can be drawn from these investigations.

The authors of the experimental work found that the single-channel diffusion rates of the univalent cations Li^+, Na^+, K^+ and Rb^+ increase with increasing mass of the migrating particles while rate-theory analysis for site-to-site diffusion predicts a decrease proportional to the square root of the mass of the particle [20,21]. An extension of the molecular dynamics simulation of the present authors [22] now indeed shows the correct trend for the mass dependence of the ion-diffusion rate. In this model the ions were allowed to move not only along the channel axis but also perpendicular to it. Van der Waals potentials for the ion-carbonyl interaction were added to the ionic potentials and a repulsive non-ionic potential was introduced at the 'walls' of the channel to prevent the escape of the ion during the numerical simulation. Although the numerical results show the correct trend for the mass dependence of the ion-diffusion rate, such 'numerical experiments' cannot give an explanation of the principle underlying this trend.

In this paper we present the results of a rate-theoretical analysis based on a model approach similar to that used in our numerical work. In section 2 the different aspects of our models are described. In section 3 a rate expression is derived including entropy phenomena while in section 4 some numerical results are presented. Some conclusions related to the general applicability of our theory are drawn.

2. Model approaches

It is the aim of this paper to find a qualitative explanation for the fact that heavier (and larger) univalent cations may migrate faster through a transmembrane channel than lighter (and smaller) ones. For this reason two different models are treated which mimic particular ion-channel interactions which play important roles in the transport process. Both models are related to those of our molecular dynamics simulations for one- and three-dimensional ionic motion in the channel. The topological properties of the model systems as well as the numerical parameters for the different parts of the interaction are in close correlation with the corresponding quantities in the gramicidin A channel.

2.1. The polar group model (model A)

In our molecular dynamics simulations, the protein channel may be treated [22] as a collection of charged and uncharged atoms and molecular

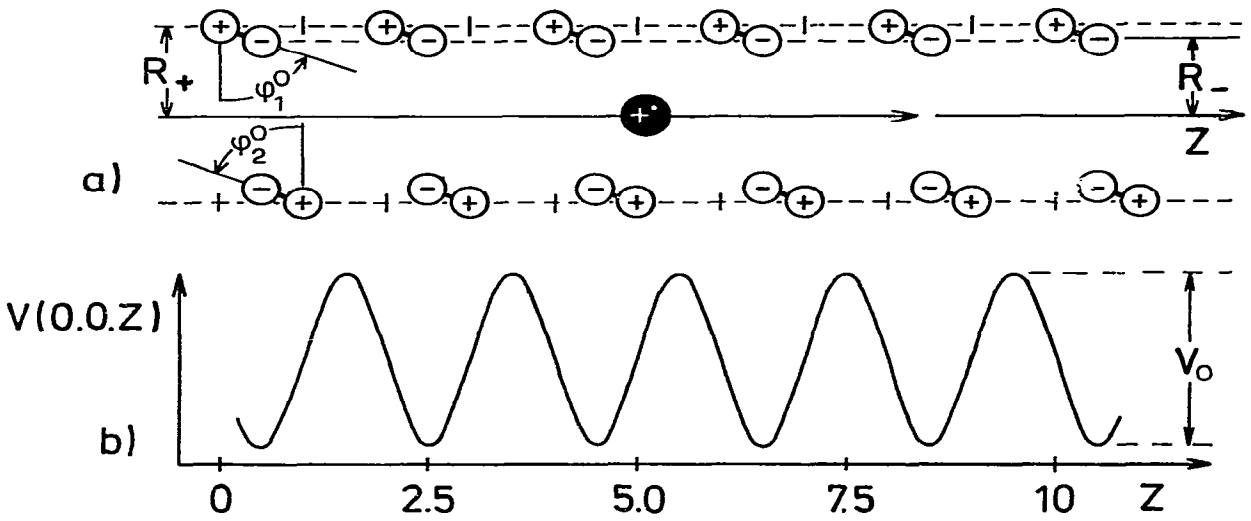

Fig. 1. (a) Arrangements of the carbonyl groups in the channel (schematically) and (b) potential energy along the channel axis z.

groups arranged near the surface of a cylinder. The details of this model, which will be referred to in this paper as model A, are described by the following statements:

(A1) The electrostatic interaction between the migrating ion and the channel is reduced to a sum of point charge interactions between polar groups (carbonyl groups) near the channel surface and the ionic charge (see fig. 1a). The positive pole of the polar group is fixed on a cylinder with radius R_+ (outer channel radius) while the negative charges are located inside the channel (distance $R_- < R_+$ from the axis).

(A2) The polar groups are assumed to occur in pairs of two dipoles, with one negative pole pointing in the forward and one in the backward direction of the channel. This model assumption is related to the gramicidin A molecule where the carbonyl groups form an alternating sequence along the helix chain (see fig. 1a).

(A3) The carbonyl groups are placed opposite one another in the channel. This arrangement differs from the one used in our molecular dynamics simulations. It was made to avoid complicated geometrical effects which are of minor importance for the understanding of the transport mechanism.

As has been demonstrated before in the one-dimensional treatment of Fischer et al. [18], the alternating arrangement of the polar groups creates a potential energy function $V(z)$ for the migrating ion along the axis (diffusion coordinate z) which is a periodic function of z with minima at positions with maximal coulombic attraction between ions

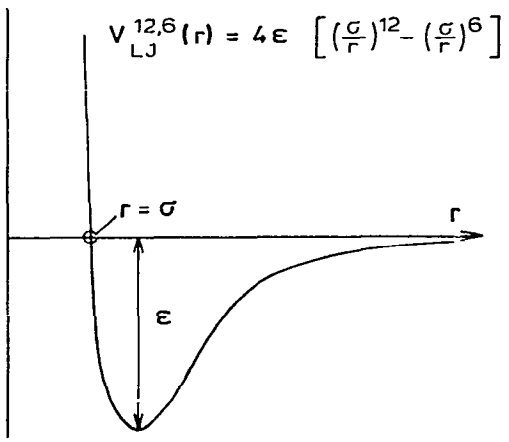

Fig. 2. Lennard-Jones (12,6) potential function for the interaction of spherical particles.

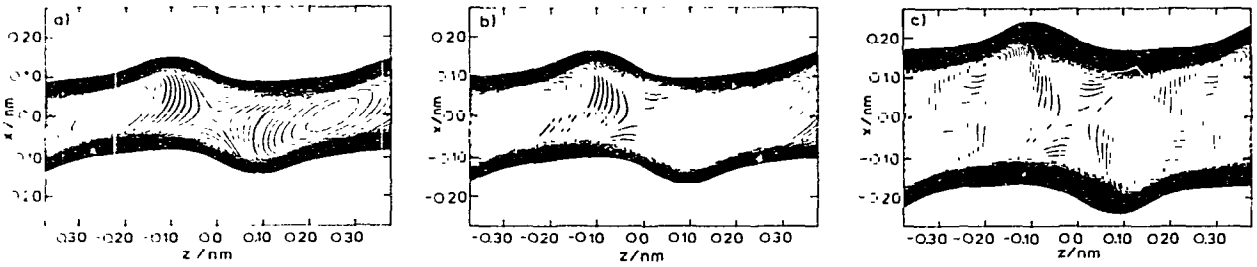

Fig. 3. Potential energy functions along the x-z plane for Rb^+ (a), K^+ (b), and Na^+ (c) in the channel of model A with $R_+ = 0.37$ nm, $R_- = 0.32$ nm and Lennard-Jones parameters of table 1.

an I polar groups and maxima at positions with maximal coulombic repulsion (see fig. 1b).

(A4) The motion of the ion is confined to the channel by introducing a repulsive interaction between the migrating particle and the cylinder surface. The repulsive potential is modelled by a d^{-12} term where d is the distance between the wall and the particle. This type of interaction takes into account the overlap of the electron distributions of two non-bonded atoms and is frequently used in Lennard-Jones (12,6) potentials (see fig. 2) for the non-ionic contributions of atom-atom and atom-molecule interactions [23]. The explicit parameters of this repulsive potential are drastically dependent on the size of the moving particles. They can be estimated using Lennard-Jones parameters for the interaction between two equivalent particles and combination rules for the repulsive potentials between different particles [24]. The details of this procedure are described in appendix A.

(A5) The non-ionic interactions between the polar groups and the ion are modelled by the Lennard-Jones (12,6) potential [23] (fig. 2):

$$V_{LJ}^{12,6} = 4\epsilon\left[\left(\frac{\sigma}{r}\right)^{12} - \left(\frac{\sigma}{r}\right)^{6}\right] \qquad (1)$$

This potential is the most common analytical potential function for non-bonding interactions of spherical particles. It has only two parameters, the range σ and the dissociation energy ϵ. σ can be roughly identified with the radius of the sphere in a hard-sphere model. The particular values for the ion-specific parameters are obtained again from standard values [23], using combination rules as

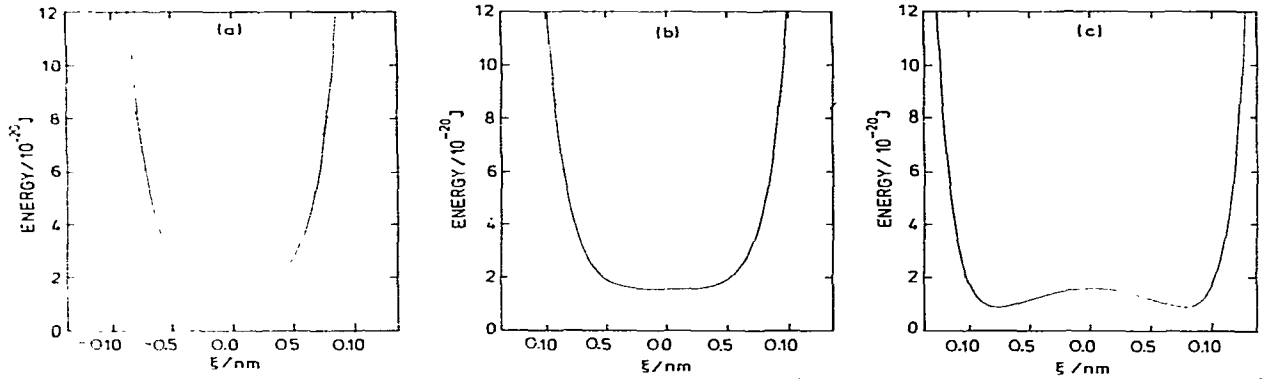

Fig. 4. Potential energy functions along ξ (perpendicular to the reaction path in the x-z plane) at the quasi-equilibrium positions (———) and the transition state (· · · · · ·) for Rb^+ (a), K^+ (b), and Na^+ (c) in model channel A. The parameters are those of fig. 3.

Table 1
Parameters for the ion-channel interaction

(A) Lennard-Jones (12,6) potentials

	σ [f]	ϵ [g]
Li^+-Li^+ [a]	2.75	0.58
Na^+-Na^+ [a]	2.94	8.10
K^+-K^+ [a]	3.46	41.70
Rb^+-Rb^+ [a]	3.62	78.40
O-O [b]	2.67	159.70
C-C [b]	3.76	132.00

(B) Partial charges for the coulomb interactions

	O [c]	C [c]	Li^+, Na^+, K^+, Rb^+
Q/e [d]	−0.38	+0.45	+1

[a] From ref. 23.
[b] From refs. 29 and 30.
[c] From ref. 31.
[d] e_0, elementary charge.
[f] As multiples of 10^{-10} m.
[g] As multiples of 10^{-23} J.

described in appendix A. As before [22,23], we used the parameter values for carbon and oxygen for the polar group atoms, in order to simulate the carbonyl groups in gramicidin A.

Two- and one-dimensional cuts through the potential energy surfaces for the migration of Na^+, K^+ and Rb^+ are drawn in figs. 3 and 4, respectively, using the parameters of table 1. Fig. 3a–c shows the potentials in the plane which contains the channel axis and the pairs of polar groups. In fig. 4a–c one-dimensional potential functions perpendicular to the diffusion coordinate at the potential minima and the 'transition' states are shown for the three ions.

Before discussing the consequences of the potential properties a second model approach is described, which is more closely analogous to a continuous description of the protein channel.

2.2. The charged-cylinder model (model B)

Instead of considering single polar groups responsible for the coulombic interaction between the ion and the channel, we now treat the channel as a medium with radial isotropy. The model assumptions can be summarized as follows:

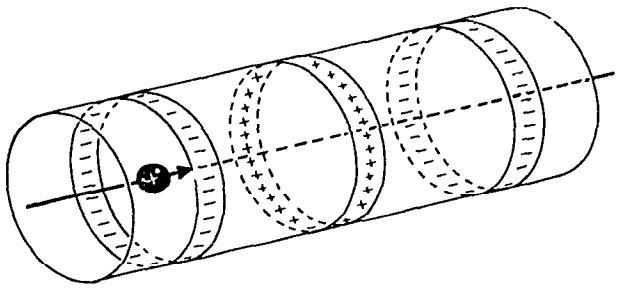

Fig. 5. Charge distribution for model channel B (schematically).

(B1) The channel has only a few quasi-equilibrium sites (minima of the potential energy along the channel axis). These sites are related to an isotropic coulomb-type attraction between the ion and the cylinder wall. Only two sites will be treated in this study (see fig. 5).

(B2) There is a radially isotropic coulombic repulsion between the ion and the channel wall (see fig. 5) at the potential maximum (transition state) separating the quasi-equilibrium sites.

(B3) As in model A, the motion of the ion is confined to the channel by introducing a repulsive interaction relative to the channel wall which is again proportional to d^{-12}. The parameters for this type of interaction are as in item A4.

(B4) The effective radius R of the channel is held constant along the axis. Its numerical value may be chosen as lying between R_+ and R_- if one wishes to compare the results of model A and model B. We have chosen $R \geq (R_+ + R_-)/2$ in some numerical treatments.

The potential energy for the ion as a function of the migration coordinate z and the distance r of the ion from the pore axis is qualitatively similar to that shown in fig. 3 but it can be treated more easily, as is demonstrated in appendix B. We can summarize that the coulombic interaction of the ion with the wall induces an ionic motion towards the axis in the transition state area, while in the quasi-equilibrium positions the ion is attracted by the wall. The combination of these coulombic potentials with the repulsive d^{-12} interaction gives the total potential. It is obvious that in the transition state area the total potential will predominantly be influenced by the coulombic potentials,

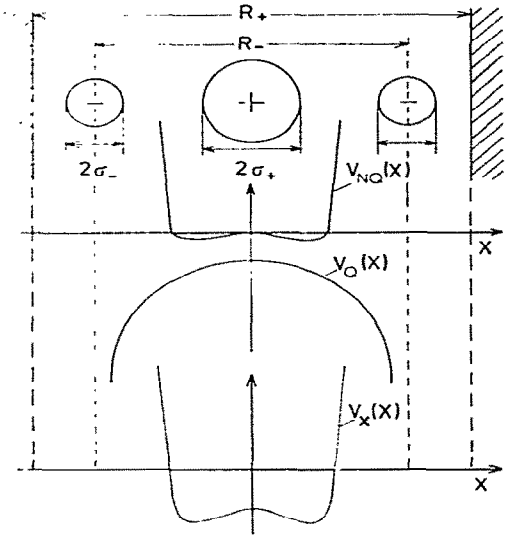

Fig. 6. Non-ionic potential $V_{NQ}(x)$, ionic contribution $V_Q(x)$ and total potential function $V_x(x)$ for the ion perpendicular to the diffusion coordinate in model A at the position of the quasi-equilibrium site (schematically).

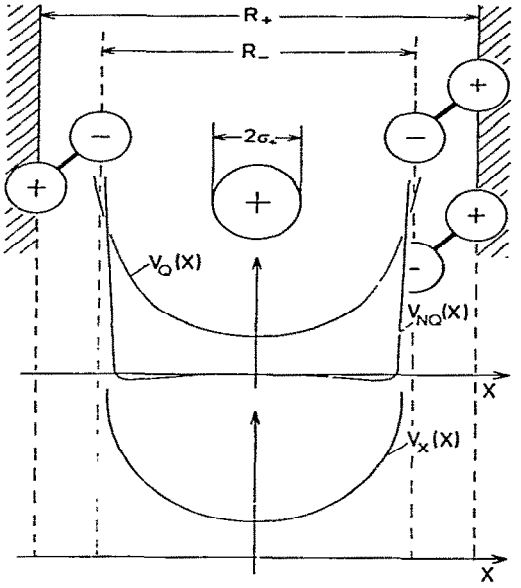

Fig. 7. Potentials $V_{NQ}(x)$, $V_Q(x)$ and $V_x(x)$ as in fig. 6 at the position of the transition state.

since these terms are long-range interactions while the d^{-12} repulsion is a short-range potential. In the minimum areas both terms contribute significantly to the total potential and the ion-specific parameters therefore play an important role here. A more detailed study of the different potential contributions is presented in the next subsection.

2.3. Consequences of the models

In both of the models presented in the preceding subsections the diffusion coordinate of the ion is nearly identical with the axis of the pore (z-axis). This assumption may not be fulfilled in real systems like the gramicidin A channel but the effect of a curvature of the reaction path (the path of steepest descent in the energy surface) on the transport rate is only significant if the particle moves over a relatively long distance (of the order of the distance between two quasi-equilibrium sites) without being influenced by interactions with the fluctuational degrees of freedom of the particles forming the channel. Such an assumption is generally not true for ion diffusion in molecular channels, as can be demonstrated using molecular dynamics simulations [18,22]. In general, there are several 'collisions' between the migrating ion and the phonons (vibrational quanta) of the channel molecule during a period of oscillation of the ion along the diffusion coordinate. Consequently, the potential models presented above can be interpreted as time-averaged potentials which can be used in statistical considerations of the diffusion process [13]. For such a concept only the partition functions of the ion at the quasi-equilibrium point and at the transition state are needed for the calculation of the rate, while deviations of the reaction coordinate from a straight line are not important. We will use the models presented above to calculate the partition functions for the motion of the ion perpendicular to the reaction path at the quasi-equilibrium sites and the transition state sites.

As can be seen from figs. 3 and 4, the potential function perpendicular to the channel axis (z-coordinate) in model A has quite different forms in the

x-direction (containing the polar groups) for the quasi-equilibrium position and the transition state position, while in the y-direction (perpendicular to the x- and z-coordinate), the two potentials are similar. We have to focus our attention on the x-coordinate, since for this coordinate strong ion-specific differences between equilibrium and transition state are expected.

The potential functions $V(x)$ along the x-coordinate contains two parts, the coulombic interaction $V_Q(x)$ and the non-ionic contribution $V_{NQ}(x)$. The qualitative forms of these parts and the total functions $V_x(x)$ can be seen from figs. 6 and 7.

At the equilibrium positions (fig. 6) the ion 'sees' an attractive coulombic force originating in the negative charges in the polar groups, i.e., the potential $V_Q(x)$ has a flat maximum value along the diffusion coordinate ($x = 0$) and decreases if the ion moves towards the channel walls along x. This motion, however, is bounded by the Lennard-Jones repulsion term of the non-ionic potential contribution $V_{NQ}(x)$. The total potential $V_x(x)$ is consequently a slight modification of $V_{NQ}(x)$, i.e., the ion can move along the x-coordinate between $\pm x_0 = \pm(R_- - \sigma_\pm)$ with relatively small variations of the potential in this region. The distance σ_{+-} can be obtained from the Lennard-Jones parameters σ_+ of the ion and σ_- of the oxygen atom by applying the Lorentz-Berthelot combination rules (see appendix B)

$$\sigma_{+-} = (\sigma_+ + \sigma_-)/2 \tag{2}$$

In the statistical treatments of the next section we will neglect the small variations of the potentials along the x-coordinate and treat the corresponding motion as free-particle motion within a box of length

$$L_x = 2R_- - \sigma_+ - \sigma_- \tag{3}$$

In model B the situation at the quasi-equilibrium sites is quite similar to that treated above. The ion now performs a quasi-free motion perpendicular to the diffusion coordinate over a distance r from the axis which is smaller than $r_0 = R - \sigma_{+-}$. Neglecting again small fluctuations of the potential the ion can oscillate within an area of

$$F_r = \pi r_0^2 = \pi(R - \sigma_{+-})^2 \tag{4}$$

At the transition state sites of model A (fig. 7), the ionic and non-ionic contributions, $V_Q(x)$ and $V_{NQ}(x)$, respectively, are of the same sign. The ion is focussed toward the center of the channel. At this position only the long-range coulombic part $V_Q(x)$ significantly contributes to the total potential function $V_x(x)$. The repulsive non-ionic interaction between the ion and the wall of the channel comes into play only for very high energies. Since the ionic parts of the potentials are independent of the sizes of the particles, $V_x(x)$ will become also independent of these. Consequently, all univalent ions see roughly the same potential along x at the transition state (see figs. 3 and 4). This potential can be modelled by a harmonic oscillator with a force constant f_x which is only dependent on the charge of the ions

$$V_x(x) = f_x x^2/2 \tag{5}$$

In model B again the situation is similar to model A. Now an isotropical potential well is formed for the motion perpendicular to the diffusion coordinate at the transition state. The force constant for this two-dimensional motion is now f_r and the potential can be modelled by a two-dimensional oscillator

$$V(r) = f_r r^2/2 = f_r(x^2 + y^2)/2 \tag{6}$$

In the next section the simplified potentials for the motion of the ion perpendicular to the reaction coordinate at the quasi-equilibrium site and the transition states will be used to calculate ion-specific diffusion rates on the basis of a rate-theoretical analysis.

3. Diffusion coefficients from rate theory

It is well known from experimental observations that most hopping diffusion processes in ordered material have an Arrhenius temperature dependence (see, e.g., ref. 25). The diffusion constant can be formally given as

$$D = D_\infty(T) \exp(-E_a/kT) \tag{7}$$

where k is Boltzmann's constant and E_a the activation energy. The pre-exponential factor $D_\infty(t)$ is in general smoothly dependent on the absolute tem-

perature T. For a mean jump length a between two quasi-equilibrium sites the diffusion coefficient D is related to the site-to-site migration rate ν by the relation

$$D = a^2\nu/2 \tag{8}$$

In a series of papers by Läuger and co-workers [9,13,19], ion diffusion in biomembrane channels was dealt with under a rate-theoretical concept similar to that of solid-state diffusion (see, e.g., refs. 25 and 26). It has recently been shown [18,22] that this concept can principally be applied to the site-diffusion process in model channels of infinite extension. In this treatment we also apply the rate-theoretical concept to calculate the site-to-site migration rate, including explicitly the characteristic model properties outlined in section 2.

In Eyring's formulation of the absolute rate theory [20,21,27,28], the rate constant of a thermally activated rate process is given by the expression

$$\nu = \frac{M^\ddagger}{M}(kT/h)\Omega^\ddagger\Omega^{-1}\exp(-V_0/kT) \tag{9}$$

where $M^\ddagger/M$ is the ratio of the number of activated states to the number of sites, k and h Boltzmann's and Planck's constant, respectively, $\Omega^\ddagger$ the partition functions of the transition state not including the reaction coordinate (diffusion coordinate), and Ω the total partition function of the equilibrium state. The value of V_0 is the difference of the potential energy between transition state and quasi-equilibrium well (see fig. 1). We will use our model properties of section 2 to estimate the partition functions $\Omega^\ddagger$ and Ω for the case of ion migration in a channel.

The total partition function Ω of the quasi-equilibrium sites can be formally given by [21]

$$\Omega = \Omega_x\Omega_y\Omega_z\prod_{i=1}^{k}\Omega_i \tag{10}$$

where Ω_x, Ω_y and Ω_z are the partition functions for the ionic motion along the x-, y- and z-direction in the minimum configuration, respectively, and Ω_i the partition functions for the ith mode of the channel vibrations. We do not know the individual Ω_i functions but we can assume – as is done in standard reaction rate theory – that these functions do not significantly change going from the quasi-equilibrium site position to the transition state position. The transition state partition function consequently can be given as

$$\Omega^\ddagger = \Omega_x^\ddagger\Omega_y^\ddagger\prod_{i=1}^{k}\Omega_i \tag{11}$$

With $M^\ddagger/M = 1$ and eqs. 10 and 11, the rate equation (eq. 9) becomes

$$\nu = (kT/h)\frac{\Omega_x^\ddagger\Omega_y^\ddagger}{\Omega_x\Omega_y\Omega_z}\exp(-V_0/kT) \tag{12}$$

For Ω_z the partition function of a harmonic oscillator along the diffusion coordinate z can be used [21]

$$\Omega_z = \exp(-\theta_z/2T)[1-\exp(-\theta_z/T)]^{-1} \tag{13}$$

with

$$\theta_z = h\nu_z/k \tag{14}$$

and ν_z being the classical frequency of oscillation of the ion along the diffusion coordinate in the equilibrium well. In the high-temperature limit $\theta_z \ll T$, this partition function becomes

$$\Omega_z' = \frac{kT}{h\nu_z}\exp[-h\nu_z/2kT] \tag{15}$$

For model A (see section 2) the partition function along the y-coordinate should not significantly differ in the equilibrium and the transition state, i.e.

$$\Omega_y \cong \Omega_y^\ddagger \tag{16}$$

since the potential functions along this coordinate are not very sensitive to the diffusion coordinate z. However, the corresponding functions along the x-coordinate drastically differ going from the site to the transition state. For the quasi-equilibrium state model A this is approximately a partition function of a one-dimensional free motion in a box of length L_x (see eq. 3) which becomes in the high-temperature (classical) limit [21]

$$\Omega_x = (2\pi mkT)^{1/2}L_x/h \tag{17}$$

The partition function $\Omega_x^\ddagger$ for motion along x at the transition state of model A can be approximated as in eq. 13 by a harmonic oscillator parti-

tion function

$$\Omega_x^{\ddagger} = \exp(-\theta_x^{\ddagger}/2T)\left[1-\exp(-\theta_x^{\ddagger}/T)\right]^{-1} \tag{18}$$

with the high-temperature form

$$\Omega_x^{\ddagger\prime} = \frac{kT}{h\nu_x^{\ddagger}}\exp(-h\nu_x^{\ddagger}/2kT) \tag{19}$$

and the classical frequency $\nu_x^{\ddagger}$ in the x-direction which can be related to the force constant f_x of the potential equation eq. 5 by

$$\nu_x^{\ddagger} = (f_x^{\ddagger}/m)^{1/2}/2\pi \tag{20}$$

With the partition function (eqs. 13–19) the total rate for the site-to-site migration (eq. 12) for model A becomes

$$\nu^{(A)} = \frac{\nu_z}{\nu_x^{\ddagger}}\left(\frac{kT}{2\pi m}\right)^{1/2} L_x^{-1}\exp\left[-\left(V_0+\frac{h}{2}(\nu_x^{\ddagger}-\nu_z)\right)/kT\right]$$

$$= \left(\frac{f_z kT}{2\pi f_x m}\right) L_x^{-1}\exp[-E_a/kT] \tag{21}$$

The activation energy is smoothly dependent on the mass of the migrating ion, since $\nu_x^{\ddagger}$ and ν_z are mass dependent (see eq. 20) but if those frequencies are of comparable magnitude E_a becomes equal to V_0. The pre-exponential factor shows the usual behaviour with respect to the mass m, i.e., $\nu^{(A)} \propto m^{-1/2}$ but there is strong dependence on the size of the ions via the parameter L_x (see eq. 4)

$$\nu^{(A)} \propto (2R_- - \sigma_+ - \sigma_-)^{-1} \tag{22}$$

This factor may cause the small ions to migrate more slowly than larger ions. From eq. 21, the ratio $R_{12}^{(A)}$ of the diffusion rates of two univalent ions with masses m_1 and m_2 and 'diameters' σ_{1+} and σ_{2+} becomes (for model A)

$$R_{12}^{(A)} = \frac{\nu_1^{(A)}}{\nu_2^{(A)}} = \left(\frac{m_2}{m_1}\right)^{1/2}\frac{2R_- - \sigma_{2+} - \sigma_-}{2R_- - \sigma_{1+} - \sigma_-}$$

$$\times\exp\left\{\frac{\hbar}{2}(f_x^{\ddagger 1/2} - f_z^{1/2})(m_2^{-1/2} - m_1^{-1/2})\right\} \tag{23}$$

with $\hbar = h/2\pi$.

If $f_x \approx f_z$, which is approximately the case in the model situations discussed in section 2, one ends up with the simple relation

$$R_{12}^{(A)} = \left(\frac{m_2}{m_1}\right)^{1/2}\frac{2R_- - \sigma_{2+} - \sigma_-}{2R_- - \sigma_{1+} - \sigma_-} \tag{24}$$

This is an important result, since it shows that there are two trends regulating the diffusion rate. These trends are in opposite directions. The normal mass effect makes a lighter ion faster than a heavier one while the size effect predicts a higher diffusion rate for larger ions. This was also found in some experiments [2,3,7,17]. In section 4 some numerical treatments are presented using the parameters from table 1 for the ions Li^+, Na^+, K^+ and Rb^+.

Before discussing the consequences of the more macroscopic model B we will give an interpretation of the surprising result of eq. 24. We will consider the molar vibrational entropy S_{vib} of the ion for a motion perpendicular to the reaction path [21]

$$\bar{S}_{vib} = R(\ln\Omega_\perp + T\mathrm{d}\ln\Omega_\perp/\mathrm{d}T) \tag{25}$$

where $\Omega_\perp$ is the partition function for ionic motion in the x-y plane. The entropy difference $\Delta\bar{S} = \bar{S}_{vib}^{\ddagger} + \bar{S}_{vib}^{o}$ can then easily be calculated using the simplified partition functions described above (see appendix C).

$$\frac{\Delta\bar{S}}{R} - \frac{1}{2} = \ln\left[\frac{2\pi kT}{f_x^{\ddagger}L_x^2}\right]^{1/2} \tag{26}$$

and the rate $\nu^{(A)}$ (eq. 21) becomes

$$\nu^{(A)} = \nu_z e^{-1/2}\exp(\Delta\bar{S}/R)\exp(-E_a/kT) \tag{27}$$

One can conclude from eqs. 26 and 27 that in the model case (A):

(i) The entropy $\Delta\bar{S}$ may have a remarkable influence on the site-to-site migration rate.

(ii) That this entropy is only a function of the size of the migrating particle but is not dependent on the particle mass, and consequently,

(iii) That for $E_a \approx V_0$ (independent of particle mass) differences in the migration rate of two particles of equal mass but different size are due only to entropy effects.

In model B the migration dynamics can be treated similarly to that of model A. Since the motion of the ion is now isotropic perpendicular to the diffusion coordinate, one has with eq. 4 analogously to eq. 17

$$\Omega_x\Omega_y = 2\pi mkTF_r/h^2 \tag{28}$$

and analogously to eq. 19

$$\Omega_z^{\ddagger}\Omega_r^{\ddagger} = \left(\frac{kT}{h\nu_r^{\ddagger}}\right)^2 \exp(-h\nu_r^{\ddagger}/kT) \tag{29}$$

which lead to an expression for the site-to-site rate (see appendix C)

$$\nu^{(B)} = \nu_z \frac{kT}{2\pi\nu_r^{\ddagger 2} m F_r} \exp\left\{-\left(V_0 + h\nu_r^{\ddagger} - \frac{h\nu_z}{2}\right)/kT\right\}$$
$$= \nu_z e^{-1} \exp(\Delta\bar{S}/R) \exp(E_a/kT) \tag{30}$$

which is formally equivalent to eq. 27. Again the entropy difference $\Delta\bar{S}$ is independent of the mass of the ions while the prefactor ν_z shows the normal $m^{-1/2}$ dependence. Neglecting again the small modification of the activation energies due to zero-point vibrational contributions, the ratio $R_{12}^{(B)}$ of diffusion rates of two univalent ions with masses m_1 and m_2 and diameters σ_{1+} and σ_{2+} becomes (for model B)

$$R_{12}^{(B)} = \frac{\nu_1^{(B)}}{\nu_2^{(B)}} = \left(\frac{m_2}{m_1}\right)^{1/2} \left(\frac{R-\sigma_{2+}}{R-\sigma_{1+}}\right)^2 \tag{31}$$

where the expression eq. 4 for F_r was used. The relation eq. 31 is equivalent to eq. 24 of model A. Again it is seen that there are two opposing trends for migration rate related to the mass m and the radius σ_+ of the ions. In section 4 some numerical examples are treated using parameters from experimental data and earlier simulational calculations.

4. Numerical results

It was demonstrated above that for both models A and B the entropy difference $\Delta\bar{S}$ between the quasi-equilibrium sites for the ions in the channel and the transition states separating these sites has an effect (in addition to the normal mass effect) on the diffusion rate which is ion-size dependent but does not depend on the masses of the migrating particles. The models are drastic simplifications of the real protein channels such as the gramicidin A dimer and their use is justified for predicting qualitative trends only if well known experimental and numerical results (from computer experiments) can be sufficiently interpreted. We tested the treatments outlined above by comparing them with the experimental data of Eisenmann and co-workers [2,3,7] and with the molecular dynamics results of the present authors [22]. For this reason we chose parameters in close agreement with those of the gramicidin A channel and calculated relative values $R_{12}^{(A)}$ (eq. 24) and $R_{12}^{(B)}$ (eq. 31) where the migration rate ν_2 of Na^+ was taken as a reference system. The ratios $R_{12}^{(A)}$ corresponding to model A are listed in table 2 together with our molecular dynamics results [22] and the experimental values of Neher et al. [2,3]. We used the ion parameters, as listed in table 1, for the numerical calculations. The effective masses of the migrating particles were chosen to be pure ionic masses or these masses plus the masses of one or two water molecules. It is seen that the trend found in experiments and numerical simulations can be sufficiently explained by the simple model approach presented in this paper. The entropy effect overcompensates for the normal mass effects (values in parentheses in table 2) and leads to a higher diffusion rate of the larger ions relative to the smaller ones. The numerical values for $R_{12}^{(A)}$ (see eq. 24) agree best with experimental data for effective masses of the migrating particles, which are larger than the pure ion masses, indicating that there is at least a partial solvation of the ions in the channel. For the smaller ion Li^+ there are relatively large quantitative differences between the observed and calculated R_{12} values, although the trend is given correctly. These deviations are due to the fact that the simplifying assumption underlying our treatments – that the ion in the quasi-equilibrium position moves in a flat anharmonic well – is probably very crude. As can be seen from fig. 3, the lighter ions tend to form a double-well potential perpendicular to the migration coordinate. If this effect is strong enough, a modification of the activation energy is expected apart from the entropy effects discussed above. We will examine this case in a subsequent article.

We also compared the results of our analytical treatments with a series of molecular dynamics results for the diffusion of a univalent ion with the mass of Na^+ but with different sizes [22] (namely, those of Li^+, Na^+, K^+ and Rb^+). No mass effects are expected and in this series, all differences in

Table 2

Ratios $R_{12} = \lambda_{X^+}/\lambda_{Na^+}$ for the ionic conductivities λ_{X^+} and λ_{Na^+} in gramicidin A-like channels for X = Li, K, Rb

X	Experimental	R_{12} from molecular dynamics simulation	$R_{12}^{(A)}$, this work, from eq. 23 [g]		
			[d]	[e]	[f]
Li	0.32 [a]				
	0.32 [b]	0.50	1.50 ± 0.03	1.05 ± 0.02	0.96 ± 0.02
	0.24 [c]		(1.82)	(1.28)	(1.17)
K	2.33 [a]				
	2.01 [b]	1.76	1.85 ± 0.35	2.04 ± 0.35	2.14 ± 0.34
	1.93 [c]		(0.77)	(0.85)	(0.89)
Rb	3.08 [a]				
	2.88 [b]	1.33	2.20 ± 0.54	2.67 ± 1.22	2.97 ± 1.35
	3.17 [c]		(0.52)	(0.63)	(0.70)

[a–c] From ref. 3 with electrolyte concentrations of 50, 100 and 300 mM, respectively.

[d–f] Calculated with effective ion masses which are the pure ion mass, the mass of the ion plus one and two water molecules, respectively. $R_- = 0.32$ nm was chosen, the error bounds are due to a variation of R_- by $\Delta R_- = 0.5$ nm.

[g] In parentheses the ratios expected from normal mass effect.

the results are only consequences of the sizes of the particles. In the molecular dynamics work, R_{12} ratios (with Na^+ as a reference ion) of 0.30, 2.24 and 2.72 are produced for Li^+, K^+ and Rb^+, respectively, while eq. 24 predicts values of 0.82, 2.40 and 4.13 for the corresponding quantities, showing again that our simplifying model is capable of predicting the correct trends.

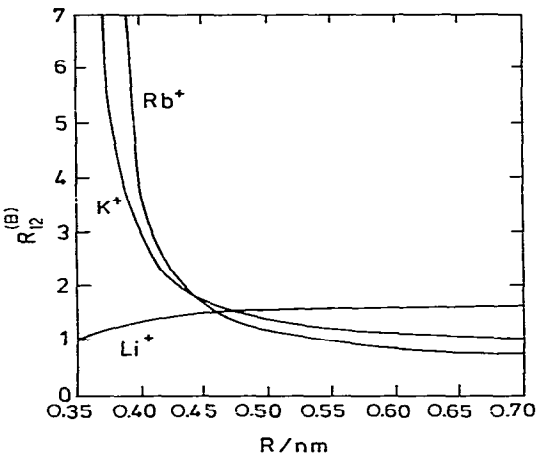

Fig. 8. Ratios $R_{12}^{(B)}$ (eq. 31) of the ion-transport rates of Li^+, K^+ and Rb^+ with respect to Na^+ as functions of the pore radius R.

We also tested model B with some numerical examples. In this case the geometric parameters of the gramicidin A channel cannot be applied directly; we have chosen the effective pore radius as $0.35\ \text{nm} \leq R \leq 0.70\ \text{nm}$. The ratios $R_{12}^{(B)}$ for the migration rate of Li^+, K^+ and Rb^+, respectively with respect to the rate of Na^+ are given in fig. 8 as a function of R. Again, drastic entropy effects are expected if the effective pore radius R decreases. The estimates produced by model B can probably better be used than those of model A in all cases where only a rough knowledge of the microscopic channel structure is available.

5. Conclusions

A model approach is introduced in this paper which takes entropy effects for the migration rates of different ions in protein channels into account. The main results and some conclusions can be summed up as follows.

(i) Analytical expressions for the ion-transport rates were derived on the basis of the rate-theoretical concept using only microscopic parameters of the channel and the migrating ions.

(ii) Numerical tests of our expressions show that not only experimental data but also the results of numerical computer simulations on the diffusion of different ions through the extensively studied gramicidin A channel are well fitted by our formulas.

(iii) We found that the inversion of the normal mass effect on the diffusion rates of different ions is mainly caused by strong entropy effects. The activation entropies can be explicitly estimated from microscopic data.

(iv) For small ions and (or) wide channels, the entropy effect is accompanied by a change of the actual activation energy comparing different ion.

Appendix A: Combination rules for Lennard-Jones (12,6) parameters

Non-ionic interactions between equivalent atoms or molecules with approximately spherical shape can be well described by Lennard-Jones-type potentials $V_{LJ}^{12,6}(r)$ (eq. 1). The parameters σ and ϵ for a neutral system are generally easily obtained from experimental sources, but the corresponding values for ions can only be determined indirectly, for instance, from alkali halide data by applying the so-called combination rules for the potentials between different partners [23]. For two parameter potentials such as a Lennard-Jones interaction, the so-called Lorenz-Berthelot rules [24] are commonly used

$$\sigma_{12} = (\sigma_{11} + \sigma_{22})/2 \qquad \text{(A1)}$$

$$\epsilon_{12} = (\epsilon_{11}\epsilon_{22})^{1/2}$$

We use averaged σ and ϵ values for the ions Li^+, Na^+, K^+ and Rb^+ and the well known parameters for C and O atoms to calculate the effective ion-channel interaction. Since the σ parameters roughly correspond to the particle radii, one can see that the additivity rule of hard spheres is sufficiently valid also in the Lennard-Jones interaction case.

Appendix B: Coulombic energy for a charged particle in a charged ring

In a single approximation the potential energy for the ion in the channel of model B can be obtained from the interaction of a uniformly charged ring of total charge Q with the particle. The partial charge of a small piece ds of the ring is then given

$$dQ = \rho ds \qquad \text{(B1)}$$

with the charge density

$$\rho = Q/2\pi R \qquad \text{(B2)}$$

and the radius R of the pore. The coulombic energy for an ion (charge q) with distance r from the axis can then be given by the integral

$$V(r) = \frac{Qq}{2\pi R}\oint ds/r' \qquad \text{(B3)}$$

where r' is the distance between the ion and a point on the ring with coordinates $R = (R, \phi)$. Simple geometric transformation yields

$$r' = [r^2 + R^2 - 2Rr\cos\phi]^{1/2} \qquad \text{(B4)}$$

and $V(r)$ becomes

$$V(r) = \frac{Qq}{2\pi}\int_0^{2\pi}\left[(R-r)^2 + 4rR\sin^2\frac{\phi}{2}\right]^{-1/2} d\phi$$

$$= 2\frac{Qq}{\pi(R-r)}\int_0^{\pi/2}\left[1 + \frac{4rR}{(R-r)^2}\sin^2\theta\right]^{-1/2} d\theta$$

$$= \frac{2Qq}{\pi(R-r)}F\left(i\frac{2(rR)^{1/2}}{R-r}\frac{\pi}{2}\right) \qquad \text{(B5)}$$

where $F(k, \pi/2)$ is the complete elliptic integral of the first kind [32]. For $Q > 0$ and $q > 0$, $V(r)$ forms a radially isotropical potential well similar to an isotropical oscillator.

Appendix C: Entropy calculations

C.1. Model A

The partition functions of the quasi-equilibrium state and the transition state for motion perpendicular to the diffusion coordinate only differ with respect to the Ω_ν contribution. For the entropy difference $\Delta\bar{S}$, consequently, only these parts are important. The corresponding molar entropies $\bar{S}_\nu$ and $\bar{S}_\nu^0$ are given from eq. 25 with eqs. 17 and 19

$$\bar{S}_x^{\circ} = R\left(\ln \Omega_x + T\mathrm{d} \ln \Omega_x/\mathrm{d}T\right)$$
$$= R\left(\tfrac{1}{2}\ln\frac{2\pi mkTL_x^2}{h^2} + \tfrac{1}{2}\right) \quad \text{(C1)}$$

and

$$\bar{S}_x^{\ddagger} = R\left(\ln \Omega_x^{\ddagger} + T\mathrm{d} \ln \Omega_x^{\ddagger}/\mathrm{d}T\right)$$
$$= R\left(\ln\frac{T}{\theta_x^{\ddagger}} + 1\right) \quad \text{(C2)}$$

The entropy difference $\Delta\bar{S}$ becomes

$$\Delta\bar{S} = \bar{S}_x^{\ddagger} - S_x^{\circ}$$
$$= \frac{R}{2}\left[\ln\left(\frac{h^2T^2}{2\pi mkTL_x^2\theta_x^{\ddagger 2}}\right) + 1\right] \quad \text{(C3)}$$

or with $\theta_x^{\ddagger} = h\nu_x^{\ddagger}/k$ the expression becomes

$$\Delta\bar{S} = \frac{R}{2}\left[\ln\frac{kT}{2\pi mL_x^2\nu_x^{\ddagger 2}} + 1\right]$$
$$= \frac{R}{2}\left[\ln\frac{2\pi kT}{f_x^{\ddagger}L_x^2} + 1\right] \quad \text{(C4)}$$

C.2. Model B

In this case the partition functions in the quasi-equilibrium site and the transition state are dependent on the x- and y-coordinate (see eqs. 28 and 29). Consequently, the corresponding entropy expressions become

$$\bar{S}_r^{\circ} = R\left[\ln(\Omega_x\Omega_y) + T\mathrm{d}\ln(\Omega_x\Omega_y)/\mathrm{d}T\right]$$
$$= R\left[\ln(2\pi mkTF_r/h^2) + 1\right] \quad \text{(C5)}$$

and

$$\bar{S}_r^{\ddagger} = R\left[\ln\left(\Omega_x^{\ddagger}\Omega_y^{\ddagger}\right) + T\mathrm{d}\ln\left(\Omega_x^{\ddagger}\Omega_y^{\ddagger}\right)/\mathrm{d}T\right]$$
$$= R\left[\ln\left(\frac{kT}{h\nu_r^{\ddagger}}\right)^2 + 2\right] \quad \text{(C6)}$$

The entropy difference becomes

$$\Delta\bar{S} = R\left[\ln\left(\frac{kT}{\nu_r^{\ddagger 2}2\pi mF_r}\right) + 1\right]$$
$$= R\left[\ln\frac{2\pi kT}{f_r^{\ddagger}F_r} + 1\right] \quad \text{(C7)}$$

Acknowledgements

We like to thank Dr. Robert Pfeiffer for carefully reading the manuscript. This work was supported by the Fonds der Chemischen Industrie, Frankfurt/Main.

References

1 S.B. Hladky and D.A. Haydon, Biochim. Biophys. Acta 274 (1972) 294.
2 G. Eisenman, J. Sandblom and E. Neher, Biophys. J. 22 (1978) 307.
3 E. Neher, J. Sandblom and G. Eisenman, J. Membrane Biol. 40 (1978) 97.
4 P. Läuger, R. Benz, G. Stark, E. Bamberg, P.C. Jordan, A. Fahr and W. Brock, Q. Rev. Biophys. 14 (1981) 513.
5 J.A. Dani and D.G. Le itt, Biophys. J. 35 (1981) 485.
6 J.A. Dani and D.G. Le itt, Biophys. J. 35 (1981) 501.
7 G. Eisenman, J. Sandblom and J. Hagglund, in: Structure and function in excitable cells, eds. W. Adelman, D. Chang, R. Leuchtag and I. Tasaki (Plenum Press, New York, 1982) in the press.
8 G. Eisenman and J.P. Sandblom, in: Proceedings of 36th international conference of Société de Chimie Physique, ed. C. Troyanowski (Elsevier, Paris, 1982) in the press.
9 P. Läuger, Biochim. Biophys. Acta 311 (1973) 423.
10 B. Hille, in: Membranes, a series of advances, vol. 3, ed. G. Eisenman (Marcel Dekker, Inc., New York, 1975) p. 255.
11 B.W. Urban and S.B. Hladky, Biochim. Biophys. Acta 554 (1979) 410.
12 J. Sandblom, G. Eisenman and J.V. Hagglund, J. Membrane Biol. (1982) in the press.
13 P. Läuger, Biophys. Chem. 15 (1982) 89.
14 D.W. Urry, Proc. Natl. Acad. Sci. U.S.A. 68 (1971) 672.
15 D.W. Urry, M.C. Goodall, J.D. Glickson and D.F. Mayers, Proc. Natl. Acad. Sci. U.S.A. 68 (1971) 1907.
16 O.S. Andersen and J. Procopio, Acta Physiol. Scand. Suppl. 481 (1980) 27.
17 O.S. Andersen, Biophys. J. (1982) in the press.
18 W. Fischer, J. Brickmann and P. Läuger, Biophys. Chem. 13 (1981) 105.
19 P. Läuger, W. Stephan and E. Frehland, Biochim. Biophys. Acta 602 (1980) 167.
20 B.J. Zwolinsky, H. Eyring and C.E. Reese, J. Phys. Chem. 53 (1949) 1426.
21 T.L. Hill, Statistical thermodynamics (Addison-Wesley, Reading, 1960).
22 W. Fischer and J. Brickmann, Ion specific diffusion rates through transmembrane protein channels: A molecular dynamics study, Biophys. Chem. (1983) submitted for publication.
23 W. Fischer and J. Brickmann, Ber. Bunsenges. Phys. Chem. 86 (1982) 650.

24 D. Henderson, Annu. Rev. Phys. Chem. 25 (1974) 461.
25 Topics in applied physics, vols. 28 and 29, Hydrogen in metals I, II, eds. G. Alefeld and J. Völkl (Springer, Berlin, 1978).
26 W. Jost, Diffusion in solids, liquids and gases (Academic Press, New York, 1952).
27 H. Eyring, J. Chem. Phys. 4 (1936) 283.
28 R.E. Powell, W.E. Rosevaere and H. Eyring, Ind. Eng. Chem. 33 (1941) 430.
29 S. Lifson and A. Warshel, J. Chem. Phys. 49 (1968) 5116.
30 A. Warshel, M. Levitt and S Lifson, J. Mol. Spectrosc. 33 (1970) 84.
31 G.E. Schulz and R.H. Schirmer, Principles of protein structure (Springer, New York, 1979) ch. 2.
32 L.M. Milne-Thompson, in: Handbook of mathematical functions, eds. M. Abramowitz and I.A. Stegun (Dower Publications, Inc. New York, 1965) p. 567.